12-15-2015

Supermassive Black Hole Seed Formation at High Redshifts: Long-Term Evolution of the Direct Collapse

Isaac Shlosman
University of Kentucky, shlosman@pa.uky.edu

Jun-Hwan Choi
University of Texas - Austin

Mitchell C. Begelman
University of Colorado - Boulder

Kentaro Nagamine
University of Nevada - Las Vegas

Right click to open a feedback form in a new tab to let us know how this document benefits you.

Follow this and additional works at: https://uknowledge.uky.edu/physastron_facpub

Part of the Astrophysics and Astronomy Commons, and the Physics Commons

Repository Citation

Shlosman, Isaac; Choi, Jun-Hwan; Begelman, Mitchell C.; and Nagamine, Kentaro, "Supermassive Black Hole Seed Formation at High Redshifts: Long-Term Evolution of the Direct Collapse" (2015). *Physics and Astronomy Faculty Publications*. 462.
https://uknowledge.uky.edu/physastron_facpub/462

Supermassive Black Hole Seed Formation at High Redshifts: Long-Term Evolution of the Direct Collapse

Notes/Citation Information

Published in *Monthly Notices of the Royal Astronomical Society*, v. 456, issue 1, p. 500-511.

Supermassive black hole seed formation at high redshifts: long-term evolution of the direct collapse

Isaac Shlosman,[1,2]★ Jun-Hwan Choi,[3] Mitchell C. Begelman[4,5]
and Kentaro Nagamine[2,6]

[1]*Department of Physics and Astronomy, University of Kentucky, Lexington, KY 40506-0055, USA*
[2]*Theoretical Astrophysics, Department of Earth and Space Science, Graduate School of Science, Osaka University, Osaka 560-0043, Japan*
[3]*Department of Astronomy, University of Texas, Austin, TX 78712-1205, USA*
[4]*JILA, University of Colorado and National Institute of Standards and Technology, 440 UCB, Boulder, CO 80309-0440, USA*
[5]*Department of Astrophysical and Planetary Sciences, 391 UCB, Boulder, CO 80309-0391, USA*
[6]*Department of Physics and Astronomy, University of Nevada, Las Vegas, NV 89154-4002, USA*

ABSTRACT

We use cosmological adaptive mesh refinement code ENZO zoom-in simulations to study the long-term evolution of the collapsing gas within dark matter haloes at z. This direct collapse process is a leading candidate for rapid formation of supermassive black hole (SMBH) seeds. To circumvent the Courant condition at small radii, we apply the sink particle method, focusing on evolution on scales ~ 0.01–10 pc. The collapse proceeds in two stages, with the secondary runaway happening within the central 10 pc. The sink particles form when the collapsing gas requires additional refinement of the grid size at the highest refinement level. Their growth is negligible with the sole exception of the central seed which grows dramatically to $M_{seed} \sim 2 \times 10^6 \, M_\odot$ in ~ 2 Myr, confirming the feasibility of this path to the SMBH. The variability of angular momentum in the accreted gas results in the formation of two misaligned discs. Both discs lie within the Roche limit of the central seed. While the inner disc is geometrically thin and weakly asymmetric, the outer disc flares due to turbulent motions as a result of the massive inflow along a pair of penetrating filaments. The filamentary inflow determines the dominant Fourier modes in this disc – these modes have a non-self-gravitational origin. We do not confirm that $m = 1$ is a dominant mode that drives the inflow in the presence of a central massive object. The overall configuration appears to be generic, and is expected to form when the central seed becomes sufficiently massive.

Key words: methods: numerical – galaxies: formation – galaxies: high-redshift – cosmology: theory – dark ages, reionization, first stars.

1 INTRODUCTION

Supermassive black holes (SMBHs) formed early in the history of the Universe. Luminous quasars have been observed up to redshifts $z \sim 7.1$ (e.g. Fan et al. 2003; Mortlock et al. 2011; Wu et al. 2015), and have been estimated to host SMBHs in excess of $10^9 \, M_\odot$, just 700 Myr after the big bang. Unless the SMBHs are primordial, they must have formed by the accumulation of matter during the epoch of galaxy formation – either as remnants of the Population III stars (e.g. Haiman & Loeb 2001; Abel, Bryan & Norman 2002; Bromm & Larson 2004; Volonteri & Rees 2006; Li et al. 2007; Pelupessy,

Di Matteo & Ciardi 2007), or the end products of gas collapse into dark matter (DM) haloes with virial temperatures $\gtrsim 10^4$ K (e.g. Haehnelt & Rees 1993; Oh & Haiman 2002; Bromm & Loeb 2003; Volonteri & Rees 2006; Begelman, Volonteri & Rees 2006; Begelman & Shlosman 2009; Milosavljević et al. 2009; Mayer et al. 2010; Schleicher, Spaans & Glover 2010; Hosokawa et al. 2011; Johnson et al. 2011; Choi, Shlosman & Begelman 2013, 2015; Latif et al. 2013; Prieto, Jimenez & Haiman 2013). Accounting for radiative feedback during formation of Pop III stars lowers their main-sequence masses to be more in line with those of normal stars. The black hole remnants are downsized as well, to $\sim 10 \, M_\odot$, making it exceedingly difficult to explain the growth of early SMBHs from Pop III seeds. Furthermore, recent results from *Planck* have pushed the beginning of the Pop III epoch forward from ~ 400 to ~ 560 Myr

★ E-mail: shlosman@pa.uky.edu

after the big bang (e.g. Planck Collaboration XIII 2015). Taken together, these arguments favour substantially more massive SMBH seeds, $\sim 10^5$–$10^7 M_\odot$, as the direct collapse models suggest.

Important details of direct collapse remain unclear, e.g. how does the process evolve when the flow becomes optically thick to internally produced radiation? How is angular momentum redistributed during the optically thick regime? Does the collapse lead to a hydrostatically supported supermassive star (SMS) – a precursor to SMBH seed formation (e.g. Begelman 2010) – or does the flow remain discy and bypass the SMS and the associated thermonuclear stage (Choi et al. 2013)?

On the other hand, we now understand some of the details of the collapse in the optically thin regime. The fragmentation of the flow is damped by the dominant gravitational potential of the host DM halo and by virial supersonic turbulence – both of which substantially increase the Jeans mass of the gas. Furthermore, the DM acts as a sink of the angular momentum from the collapsing gas, both in isolated collapse models and in the cosmological context (e.g. Wise, Turk & Abel 2008; Begelman & Shlosman 2009; Choi, Shlosman & Begelman 2013, 2015).

Studies of the direct collapse to form the SMBH seeds involve computationally intensive efforts to follow the hydrodynamics and the thermal state of the collapsing gas. Processes like fragmentation, star formation, redistribution of angular momentum in the collapsing flow, development of a supersonic turbulence, etc., can be addressed only numerically.

Typically, the collapse region extends over many orders of magnitude in radius, from a few kpc down to ~ 1–100 au. Even sophisticated methods face difficulties in dealing with such an extended dynamic range. As the collapse progresses, the simulation timesteps become increasingly short, making it prohibitively expensive to follow the evolution. Moreover, the build-up of the optical depth in the flow can fully or partially trap the radiation produced *in situ*, affecting the dynamics and thermodynamics of the collapsing gas.

Two options have been proposed to overcome these obstacles. The first involves (consecutive) zoom-in simulations typically associated with calculations of cosmological structure formation and galaxy evolution (e.g. Becerra et al. 2015). This method allows one to increase the mass and spatial resolution of the model, especially on the smallest scales, to introduce various physical processes, on different scales, and to avoid artefacts associated with a small number of particles or grid cells at small radii. Becerra et al. (2015) have assumed that the radiative cooling becomes inefficient at some presumed radius. Such an exponential cutoff in the cooling rate naturally leads to a radiation pressure-dominated entity – an SMS. By itself this does not resolve the issue of radiation trapping in the flow – in a 3D rotation-dominated inflow the radiation, in principle, can escape. It does not allow one to study the optically thin-to-thick transition in the flow and the nature of the flow inside the optically thick region. Merely increasing the mass and spatial resolutions will not resolve the problem and will not allow one to prolong the simulation without also introducing additional physical processes such as radiative transfer and associated dynamical effects. At present time, sufficiently powerful radiation hydrodynamics codes are not generally available.

The second option involves the sink particle method, successfully applied to star formation and other problems to focus on a specific range in radius, preventing the smaller scales from forcing an increasingly small timestep, and thus enabling one to follow the long-term evolution of the collapsing flow (e.g. Bate, Bonnell & Price 1995; Krumholz, McKee & Klein 2004; Federrath et al. 2010; Wang et al. 2010; Teyssier et al. 2011; Gong & Ostriker 2013).

In this method, gas on small spatial scales is replaced by the sink particles, which can grow in mass as the surrounding gas evolves.

In this paper, we apply the sink particle method to the direct collapse problem in a cosmological framework. We focus on the long-term evolution of the flow and on associated processes on scales of ~ 0.01–10 pc, deep inside the DM halo gravitational potential. The choice of this scale is based on purely numerical reasons, in order to circumvent the exceedingly small timestep. It also allows us to avoid additional physical processes on the small scale, such as radiative transfer, without any loss of generality.

Starting with our cosmological simulations of direct collapse (Choi et al. 2015), we create sink particles in the flow (as described in Section 2), and analyse motions and growth of these particles and their effect on the collapse itself. Choi et al. has followed the collapse down to $\sim 10^{-4}$ pc scales, where one anticipates trapping of the continuum photons produced in the flow and the formation of a photosphere. Of course, the Lyman α photons are trapped or at least partially trapped already at larger radii. Here we ignore scales smaller than ~ 0.01 pc, which allows us to continue following the collapse on scales > 0.01 pc, over time-scales much longer than those simulated by Choi et al.

This paper is structured as follows. Section 2 provides the details of our numerical technique and explains the sink particle method implemented here. We present our results in Section 3 and discuss them in the last section.

2 NUMERICAL TECHNIQUES

2.1 Simulations

We use the Eulerian adaptive mesh refinement (AMR) code ENZO-2.3, which has been tested extensively and is publicly available (Bryan & Norman 1997; Norman & Bryan 1999; Bryan et al. 2014). ENZO uses a particle-mesh N-body method to calculate the gravitational dynamics, including collisionless DM particles, and a second-order piecewise parabolic method (Bryan et al. 1995) to solve hydrodynamics. The structured AMR used in ENZO places no fundamental restrictions on the number of rectangular grids used to cover some region of space at a given level of refinement, or on the number of levels of refinement (Berger & Colella 1989). A region of the simulation grid is refined by a factor of 2 in length scale, if either the gas or DM density becomes greater than $\rho_{0,\,\text{gas, dm}} N^l$, where $\rho_{0,\,\text{gas, dm}}$ is the cosmic mean density for the gas or DM, respectively, $N = 2$ is the refinement factor, and l is the maximal AMR refinement level.

The Jeans length has been resolved by at least 16 cells in the simulations. Hence, the Truelove et al. (1997) requirement for resolution of the Jeans length (see Section 2.3), i.e. at least four cells, has been superseded substantially (e.g. Sur et al. 2010; Federrath et al. 2011; Turk et al. 2012; Latif et al. 2013).

ENZO follows the non-equilibrium evolution of six species: H, H$^+$, He, He$^+$, He^{++}, and e^- (Abel et al. 1997; Anninos et al. 1997) in a gas with a primordial composition. It calculates radiative heating and cooling following atomic line excitation, recombination, collisional excitation and free–free transitions. Radiative losses from atomic cooling are computed in the optically thin limit.

Several radiation processes which prevent H$_2$ formation in the collapsing flow have been proposed (e.g. Omukai 2001; Spaans & Silk 2006; Schleicher, Spaans & Glover 2010; Latif, Zaroubi & Spaans 2011; Choi, Shlosman & Begelman 2013; Inayoshi, Omukai & Tasker 2014; Sugimura, Omukai & Inoue 2014). In this work,

we assume that H$_2$ does not form and exclude the chemistry and cooling related to H$_2$, which simplifies the chemical evolution.

2.2 Zoom-in initial conditions

We follow the long-term dynamical evolution of the collapsing gas within a DM halo in a fully cosmological environment and subject to atomic cooling. To satisfy the resolution requirement, we use the MUSIC code (Hahn & Abel 2011) to generate the cosmological zoom-in initial conditions (ICs). MUSIC uses a real-space convolution approach in conjunction with an adaptive multigrid Poisson solver to generate highly accurate nested density, particle displacement, and velocity fields suitable for multiscale zoom-in simulations of structure formation in the universe.

Generating a set of 'zoom-in' ICs is a two-step process. First, we generate $1h^{-1}$ Mpc comoving 128^3 DM-only ICs for the pathfinder simulation and run it without AMR until $z = 10$. Using the HOP group finder (Eisenstein & Hut 1998), we select an appropriate DM halo, whose mass is $\sim 10^8\,h^{-1}\,\mathrm{M}_\odot$ at $z = 10$. Secondly, we generate $1h^{-1}$ Mpc ICs with 512^3 resolution in DM and gas in the zoom-in region. Since we use the same random seeds of these ICs as the ICs at the first step, the phases of both ICs are identical. The zoom-in region is centred on the selected halo position and is set to be large enough to cover the initial positions of all selected halo particles.

The ICs are generated using *WMAP*5 cosmology: $\Omega_\Lambda = 0.721$, $\Omega_\mathrm{m} = 0.279$, $\Omega_\mathrm{b} = 0.0445$, $h = 0.701$, $\sigma = 0.807$, and $n_\mathrm{e} = 0.961$. In the following, we use R for spherical coordinates and r for cylindrical ones.

2.3 Sink particle algorithm

Sink particles are used in order to weaken the Courant conditions restrictions on the timestep. The restriction can result from the increase in the local density of the gas and demand for additional refinement (i.e. spatial resolution). Under these circumstances, it is nearly impossible to study the large-scale, long-term evolution of the direct collapse within DM haloes. To circumvent these numerical obstacles, we adopt the sink particle method to model the gravitational collapse. This is especially relevant for the present work, which aims at long-term evolution of the direct collapse. Before the gas density exceeds that of the DM density, at $t \sim 350$ Myr, sink particles are not used. However, after the gas decouples, its central density increases rapidly. Below we describe the specifics of this method.

Various works have invoked sink particles in order to advance their goals (e.g. Bate et al. 1995; Krumholz et al. 2004; Federrath et al. 2010; Wang et al. 2010; Teyssier et al. 2011; Gong & Ostriker 2013). We implement the sink particle method largely based on Wang et al. (2010), who studied massive star formation using ENZO AMR simulations. We require a sink particle to form when the cell violates the refinement criterion at the highest refinement level in the collapsing part of the flow.

When this happens, a sink particle is inserted at the centre of the cell. The initial sink particle mass is computed based on the mass exceeding the maximum allowed density at a maximum refinement level. In other words, each cell density has a maximal value that does not violate the refinement criterion. The initial sink particle velocity is calculated based on linear momentum conservation.

After a sink particle is formed, it accretes the gas from its host cell according to following prescription:

$$\dot{M}_\mathrm{sp} = 4\pi \rho_\mathrm{out} r_\mathrm{B}^2 \sqrt{1.2544 c_\mathrm{cell}^2 + v_\mathrm{rel}^2}, \tag{1}$$

where $\dot{M}_\mathrm{sp}$ is the mass growth rate of a sink particle, $\rho_\mathrm{out} = \rho_\mathrm{cell} \min[1.0,\ (l_\mathrm{cell}/r_\mathrm{B})^{1.5}]$, l_cell is the cell size, $r_\mathrm{B} = GM_\mathrm{sp}/(c_\mathrm{cell}^2 + v_\mathrm{rel}^2)$ is the Bondi accretion radius, c_cell is the sound speed in the cell, and v_rel is the relative velocity between the host cell and the sink particle.

Merging between sink particles is a necessary process in order to accurately estimate their mass growth rate and to reduce the computational cost. In principle, the sink particles represent overdense gas clumps in our simulations whose internal evolution we ignore. We require two sink particles to merge when their separation becomes smaller than $5l_\mathrm{cell}$, and assume that the less massive sink particle merges with the more massive one. The merging process is quite insensitive to the definition of the critical separation between particles (e.g. Wang et al. 2010). We have confirmed this by comparing various maximal refinement levels.

In this paper, we use three different maximum refinement levels that affect the overall simulation resolution and the scale of the sink particle formation. The maximal AMR refinement level l (see Section 2.1) is 10 in run L10, $l = 12$ in run L12, and $l = 15$ in run L15. The maximal spatial resolution corresponds to ~ 0.1 pc for run L12 and to ~ 0.01 pc for run L15.

All three simulations have been restarted from the cosmological run described in Choi et al. (2015), at $t \sim 355$ Myr, when the refinement level in the gas is $l = 8$, and when the gas-to-DM density ratio in the central ~ 10 pc is about unity. They are identical simulations except for the maximal AMR level. While our analysis here is based on run L12, we use runs L10 and L15 to test convergence of the observed evolution.

3 RESULTS

The DM halo under investigation has been selected from a computational box containing several such objects at $z = 10$. This halo has been resimulated at high resolution down to $z \sim 12$, or $t \sim 355$ Myr from the big bang, when it reached the virial mass and radius of $M_\mathrm{h} \sim 2 \times 10^7 h^{-1}\,\mathrm{M}_\odot$ and $R_\mathrm{vir} \sim 10 h^{-1}$ kpc in comoving coordinates, with a cosmological spin parameter $\lambda \sim 0.03$. At this time, the DM density profile can be approximated by an NFW profile (e.g. Navarro, Frenk & White 1997), with a characteristic scale radius of $R_\mathrm{s} \sim 30$ pc, in physical coordinates, and with a concentration parameter $c \equiv R_\mathrm{vir}/R_\mathrm{s} \sim 25$. At about $t \sim 355$ Myr, the gas-to-DM density ratio exceeds unity interior to $\sim R_\mathrm{s}$. The gas density quickly establishes a density profile slightly steeper than $\sim R^{-2}$, down to the limiting radius of $R \sim 10^{-4}$ pc, imposing a tight Courant condition on the timestep.

As shown by Choi et al. (2013, 2015), direct collapse, in both the isolated case and in a cosmological framework, can be divided into two parts: the first stage ends when the central gas density reaches that of the DM, and the second stage begins when the central gas density exceeds that of the DM, and the gas effectively decouples from the DM. During the latter stage, an r^{-2} density profile is established all the way down to $\sim 10^{-4}$ pc – the region where the optical depth to continuum radiation produced by the accretion flow becomes larger than unity, the so-called thin-to-thick transition. As such a large dynamic range imposes a very strict condition on the timestep, and because we focus on the optically thin part of the flow, we introduce sink particles based on the criteria discussed in Section 2.3. By doing this, we remove the smallest spatial scales, $r < 0.1$ pc (for run L12) and < 0.01 pc (for run L15), from consideration. Hence, these are the limiting resolutions of the
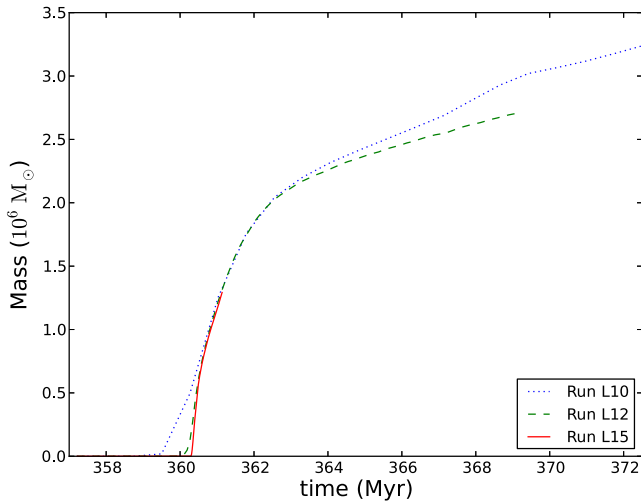
Figure 1. Evolution of the central sink particle mass, $M_{\rm seed}$, forming at the position of the density peak for three different AMR runs, L10, L12, and L15. While L10 exhibits a somewhat slower or faster growth of the central seed at various times, L12 and L15 show virtually no difference. Note, that the initial growth of the seed mass is very rapid, so that it reaches $M_{\rm seed} \sim 2 \times 10^6\,{\rm M_\odot}$ in $\lesssim 2$ Myr.

models. On the other hand, we gain the ability to follow the collapse well beyond the time achieved in Choi et al. (2015).

3.1 Rapid growth of the central sink particle

The masses of sink particles introduced in the run L12 correspond to the gas mass of the smallest grid cells. Runs L10 and L15, in this respect, are very similar, but their resolutions are ~ 1 and ~ 0.01 pc, respectively. So, the newly born particles provide only a negligible effect on the flow when they are introduced. They can grow by accretion and merging and, at least in principle, their influence grows. We find that sink particles appear always within the central ~ 1–2 pc, measured from the densest gas cell. Their number never substantially exceeds ~ 10 in the collapsing flow. They grow, but their individual masses stay below $\sim 10^3\,{\rm M_\odot}$. The sole exception is the sink particle that lies at the centre. This particle grows fast, and in less than ~ 2 Myr surpasses $M_{\rm seed} \sim 2 \times 10^6\,{\rm M_\odot}$, as shown in Fig. 1. (We term this sink particle as a 'seed' and conjecture that its evolution is closely related to the future formation of the SMBH seed.) After this time, its growth rate saturates substantially. We separate these phases into dynamic and secular growth stages of the central seed.

For comparison, we also show the evolution of the central sink particle in runs L10 and L15. In run L10, the central sink particle starts to grow slightly earlier, but very quickly its growth curve merges with that of L12, even before the end of the dynamic stage. During the secular stage, the L10 growth rate initially exceeds that for L12. Asymptotically, the L10 and L12 growth rates are nearly identical, but the final seed masses differ by about 20 per cent.

Run L15 displays a nearly identical growth for the central particle, except for very early times – growth is triggered slightly later but the rate is higher. We therefore, conclude that the resolution of run L12 is sufficient for our purpose, because the growth rates in L12 and L15 appear identical.

So, irrespective of the resolution we choose for the sink particles, the central seed grows in a very short time to exceed $10^6\,{\rm M_\odot}$. How

is this mass converted into the SMBH seed is a subject for future research.

3.2 The central massive seed and disc formation

To understand the specifics of the growth of the central seed, we plot the evolution of the gas masses within the central 2 and 20 pc, and compare them with the mass of the central seed, the total mass of other (off-centre) sink particles, and the DM within these spherical volumes. Note that the sink particles grow only by accreting gas and incorporating other sink particles, but not through accretion of DM. The total baryonic mass, i.e. the gas and the sink particles, is, therefore, conserved.

In Fig. 2(a), we observe that the total mass of the off-centre sink particles in the region remains very small. The gas accumulation inside the innermost 2 pc starts around 358 Myr and peaks at ~ 360 Myr, prior to and concurrently with the formation and rapid growth of the central seed. After the rapid growth stage, the gas mass inside this region is remarkably constant at $\sim 10^4\,{\rm M_\odot}$, showing that *net* inflow into this region is negligible. Below, we discuss the detailed mass balance in the region. Note, that the gas at the peak inflow rate into this region drags in the DM, which dominates the gas mass during the secular evolution of the central sink. This provides additional stability against the gas fragmentation in the region.

The mass evolution within the central 20 pc paints a similar picture, with an important difference (Fig. 2b). The gas mass grows monotonically until the formation of the central seed, then drops by an order of magnitude during the 2 Myr rapid growth of the central seed. This explains the source of the mass in this seed. After this time, the gas mass continues to accumulate at nearly the original rate. The DM here experiences the same adiabatic contraction as in Fig. 2(a), and dominates the gas. It is clear, however, that the gas will shortly reverse this situation – as shown by Fig. 2(b), about 10 Myr after the formation of the central seed, the gas mass in the region will surpass that of the DM, yet it will remain well below the mass of the central seed. We discuss reasons for the gas evolution in the vicinity of the central seed and its global consequences below and in Section 4.

The differences between gas evolution inside the central region and on larger scales is related to the gas kinematics. This is seen in Fig. 3, where the slope of the gas density within the central ~ 10 pc, $\rho \sim r^{-\alpha}$, changes from $\alpha \sim 2$ to ~ 0.5 – the gas density profile has flattened. Because we assume that the gas is optically thin, the temperature profile remains the same as shown in Choi et al. (2015).

Another by-product of the change in the prevailing kinematics is the evolution of the gas accretion rate profile. The peak accretion rate of $\sim 1\,{\rm M_\odot}\,{\rm yr^{-1}}$ inside ~ 10 pc is reached between $t \sim 360$ and 362 Myr (Fig. 4). This is reflected in the very fast growth of the central seed during these 2 Myr. Immediately after this, the radial profile of the mass accretion rate, $\dot{M}(r)$, drops dramatically from its peak by about two orders of magnitude or more with decreasing radius. That is, at $r \sim 10$ pc, the mass inflow rate stays approximately the same, $\sim 0.3\,{\rm M_\odot}\,{\rm yr^{-1}}$, but it declines sharply with radius to $\sim 3 \times 10^{-3}\,{\rm M_\odot}\,{\rm yr^{-1}}$ at ~ 0.3 pc. Note, that substantial amount of gas, $\sim 6 \times 10^6\,{\rm M_\odot}$, resides in the DM halo outside 20 pc at the time of disc formation, and that the accretion rate on to the halo remains high as well.

This behaviour in the gas density profile and its accretion rate within the central 20 pc means that the gas accumulates there at rapid pace. At around $t \sim 360$ Myr, this is related to the formation and a rapid growth of the central seed. However, after $t \sim 362$ Myr, this is
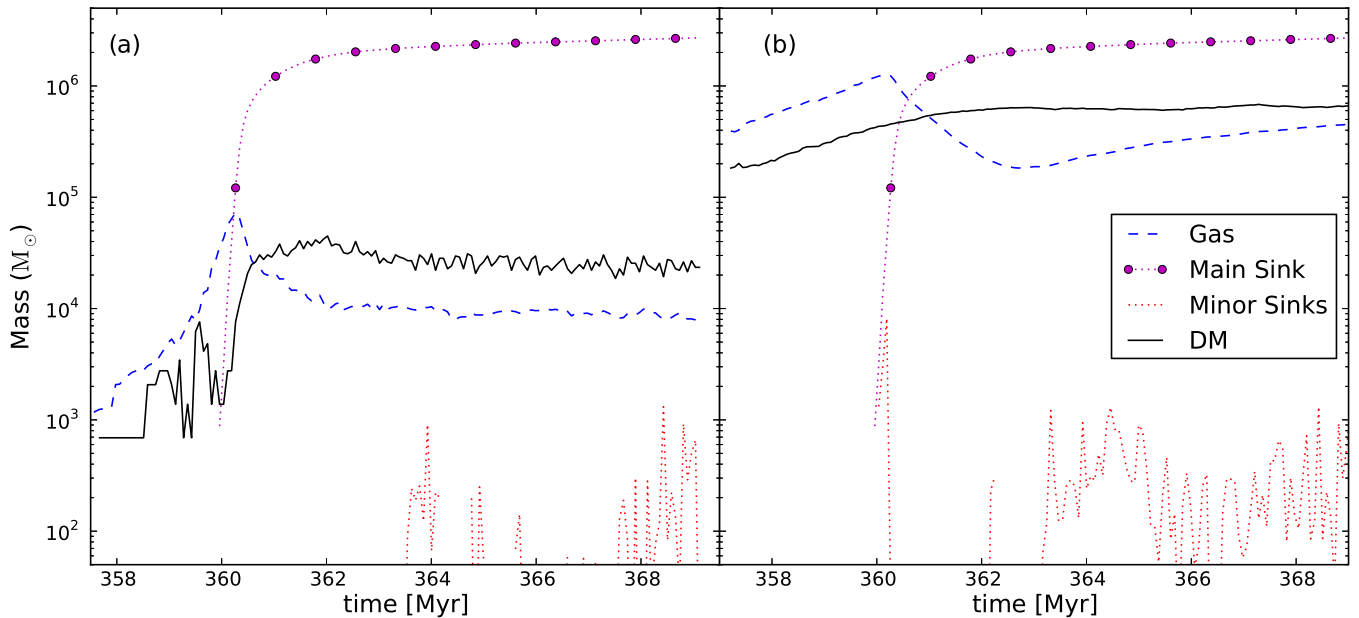
Figure 2. Evolution of masses within spherical volumes with a radius of 2 pc (left frame) and 20 pc (right frame). Shown are the gas mass (blue dashed line), DM mass (black solid line), central seed (dotted line with large dots), and the total of all minor sink particles (dotted green line).
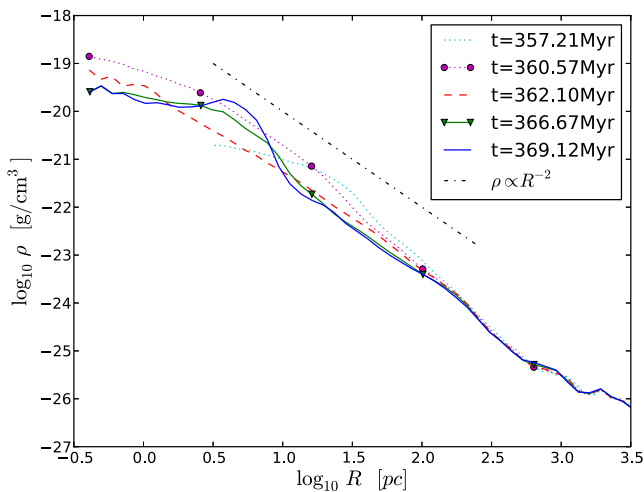

Figure 3. Evolution of the gas density profile for run L12. The density profiles, $\rho \sim r^{-\alpha}$, exhibit flattening in the central region, from $\alpha \sim 2$ to $\alpha \sim 0.5$, where the gas assembles into a disc structure around the central massive seed.
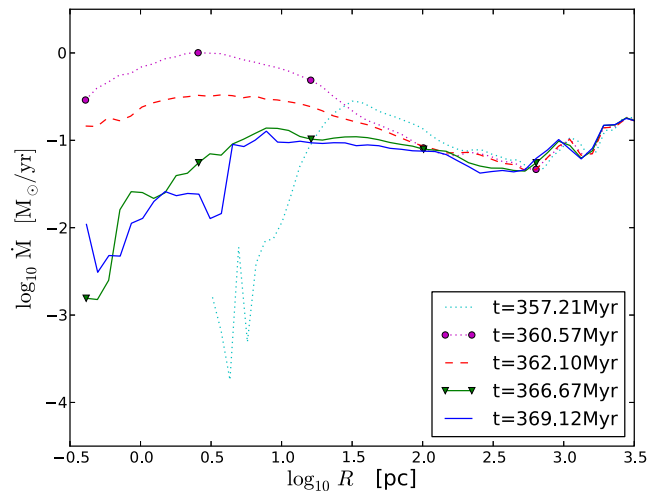

Figure 4. Evolution of the mass accretion rate profile for the L12 run. Note the sharp decrease in $\dot{M}$ from the peak of ~ 0.3–$1\,\mathrm{M_\odot}\,\mathrm{yr}^{-1}$ by about two orders of magnitude at smaller radii, as a result of the rotational support achieved near the massive sink particle.

the direct consequence of the accumulation of angular momentum and formation of a gaseous disc in this region.

Evolution of the mass accretion rate is clearly reflected in the abrupt collapse of the gas and formation of the central seed, and can be followed in the top frame of Fig. 5. The radial velocity at $t \sim 360.6$ Myr increases to $\gtrsim 70\,\mathrm{km\,s^{-1}}$. This is well above the virial velocity of the DM halo, by almost an order of magnitude, and can only result from the gravitational decoupling of the gas from the background DM potential. Rotational velocity around 0.3 pc from the central seed has reached $v_t \sim 160\,\mathrm{km\,s^{-1}}$ by $t \sim 363.6$ Myr – exceeding the DM virial velocity by a factor of ~ 16 (Fig. 5, bottom frame). Hence, the depth of the potential well due to the massive seed has substantially surpassed that in the DM. Basically, this cor-

responds to the following sequence of events: onset of gravitational collapse in the gas on scales $\lesssim 20$ pc, gravitational decoupling of the gas from the DM, formation of the massive seed, and continuing accretion on to this seed. At the same time, the increased rotational support for the gas can be clearly observed in a decreased radial inflow velocity to $v_r < 10\,\mathrm{km\,s^{-1}}$, and a corresponding sharp increase in the tangential velocity, v_t, which develops a Keplerian profile inside the inner $r \sim 50$ pc, as seen in Fig. 5.

The central seed has reached $M_{\mathrm{seed}} \sim 10^4\,\mathrm{M_\odot}$ at $t \sim 360.1$ Myr. Strong compression of the collapsing gas, shocks, and radial filaments can be observed at this time. The disc first becomes visible at ~ 361.5 Myr, when $M_{\mathrm{seed}} \sim 1.6 \times 10^6\,\mathrm{M_\odot}$, and can be seen in two out of three projection planes, xz (face-on) and xy (edge-on), initially
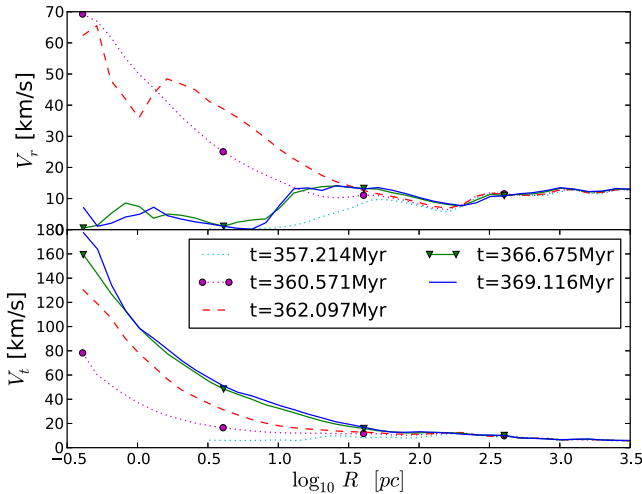
Figure 5. Evolution of the radial (top) and tangential (bottom) velocity profiles, v_r and v_t, in the gas for run L12. Note the sharp decrease in the central v_r and increase in the v_t there – a clear sign of disc formation.

on scales of the inner 2–3 pc. It grows rapidly in size, as a strong gaseous bar with two associated *open* spirals[1] become dominant around $\sim$362.1 Myr. By $\sim$362.7 Myr, the disc radius has reached $\sim$5 pc. Around $\sim$363.7 Myr, one starts to distinguish between an inner, geometrically thin disc, 2–3 pc in radius, and an outer, much thicker disc, which is misaligned by about 45° with inner one. The overall radius of this configuration is about 10–12 pc. Formation of the outer inclined disc is the result of gas influx with a different direction of angular momentum into the region.

The stages of direct collapse are depicted schematically in Fig. 6. Stage A of the collapse corresponds to the initial inflow into the DM halo. Stage B corresponds to the gas density exceeding that of the DM and dynamically decoupling from the background DM potential. Stage C culminates with the formation of the central seed and its runaway growth, and the last stage is associated with the formation of the misaligned disc system due to the fluctuating angular momentum of the accreting gas.

This configuration, of inner and outer discs being strongly misaligned, appears stable for the next $\sim$6 Myr – a time period which corresponds to about 20–25 rotational periods at $\sim$15 pc. By the end of the simulation, $t \sim$ 369.12 Myr, the inner disc has a radius of 3–4 pc and the outer disc about 10–12 pc (Fig. 7). The thickness of the inner disc is $\lesssim$1 pc, and that of the outer disc varies from $\lesssim$1 to $\sim$3 pc – this disc flares as seen in Fig. 8 (bottom frames). The inner disc is connected to the outer one with a clearly visible symmetric, integral-shaped warp.

We do not observe any fragmentation in the inner and outer discs. Why is the fragmentation suppressed in the discs, where a high-density, low-temperature gas resides? The answer to this question can be found in Fig. 2(a). After the formation of the massive central seed, the gas inflow into the central 2 pc is minimal, while $\dot{M}$ is high into the outer disc (see also Fig. 4). The mass within the region, $R \lesssim$ 20 pc, is dominated by the central seed and by the DM that was dragged inwards by collapsing gas, in adiabatic contraction. The ratio of the gravitational acceleration due to the gas to that of the central seed, $M_{gas}(<R)/M_{seed}$ is $<10^{-2}$ for the inner disc and $<10^{-1}$ for the outer disc, even at the end of the simulation.

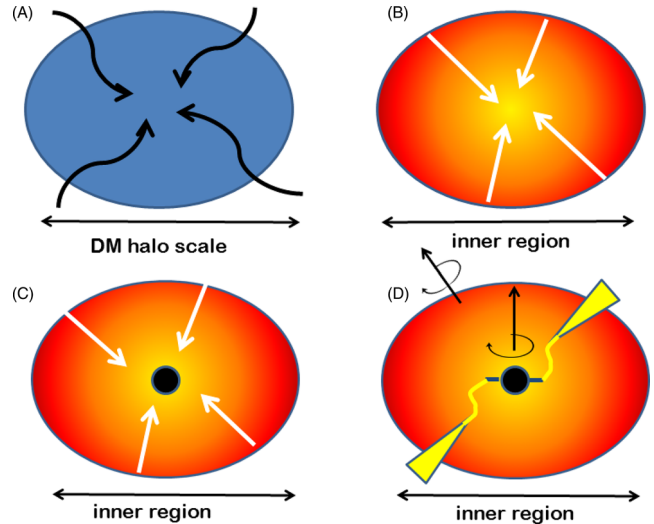[1] Such spirals signal efficient angular momentum loss by the gas.

Figure 6. Schematic picture of various stages in the direct collapse with the rapidly growing central seed. Stage A: filamentary inflow into the DM halo on scale of $\sim$1 kpc. Stage B: gas density exceeds the DM density and the secondary collapse is triggered. In the case of current simulation setup, the 'inner region' indicates roughly 20 pc region from the sink. Stage C: central sink forms and rapidly grows to $\sim$10^6 M$_\odot$. Stage D: high angular momentum gas accumulates in a system of misaligned discs (shown here edge-on), forming due to the fluctuating angular momentum of the collapsing gas. The small inner disc is shown horizontal, and the outer disc is inclined. The discs are connected by a symmetric warp. See also Fig. 8 and explanations in the text.

The necessary condition for the gas to collapse in the presence of a tidal field is that its density has to exceed the mean density associated with the tidal field. In our case, this leads to the Roche limit radius of $\sim$10 pc. Moreover, Toomre's parameter $Q \gg 1$ in both discs, due to the presence of the central seed, and the cooling floor temperature of atomic gas. The penetrating filaments also inject gas and stir turbulent motions in the outer disc (Fig. 9). So, at least for $\sim$10 Myr after the formation of the seed, and until the gas builds up anew in the region (Fig. 2b), the fragmentation in the discs will be heavily suppressed.

To visualize the morphology of the gas inflow, we produce density slices in three projection planes, xy, yz, and xz, using nested boxes, from 4 kpc on a side to 10 pc, at $t \sim$ 369 Myr (Fig. 8). The inner and outer discs are visible in the last two frames, i.e. 40 and 10 pc. The inner disc is geometrically thin and seen edge-on in the xy and yz planes and face-on in the xz plane. It is surrounded by the geometrically thicker disc, whose mid-plane is inclined to that of the inner disc by about 45° in the yz plane. Spiral structure is clearly observed in both discs. The accreting gas is shocked at the disc surface, as can be seen in the bottom frames of Fig. 9 (left and middle columns). Similar behaviour has been observed by Choi et al. (2013) for isolated models of direct collapse.

3.3 Evolution of angular momentum in the accretion flow: understanding the dynamical consequences of the massive seed

An alternative way to view the growing disc in the centre is to study the evolution of the angular momentum in the collapsing flow (Fig. 10). We show the specific angular momentum profile, $j_{gas}(r)$, at four representative times. For comparison, we also plot the circular
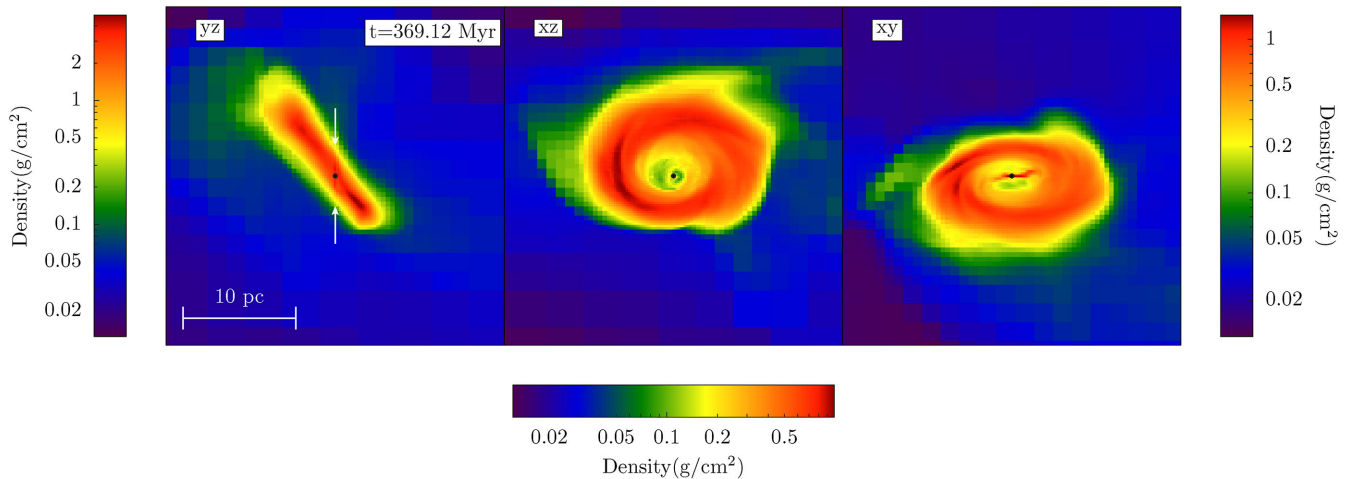
Figure 7. Gas column density normal to main planes at the end of the simulation, $t \sim 369$ Myr, for run L12. The left frame shows the inner edge-on disc (position delineated by the white arrows) embedded in the outer disc which is inclined by about 45° in the *yz* plane. The middle frame shows the same figure with the inner disc being face-on in the *xz* plane. The right frame shows another projection of the inner edge-on disc and the inclined (towards the observer) outer disc in the *xy* plane. The inner warp connection between the discs can be clearly seen in this projection. The position of the central seed is shown by a black point. The filaments which feed the outer disc are clearly visible.

angular momentum profiles, $j_c(r)$. Initially, the gas has $j_{gas} \ll j_c$, but increases its specific angular momentum with time, as more gas starts to move inwards. For $t = 365.9$ Myr, the gas inside ~ 10 pc radius from the seed exhibits a nearly maximal allowable rotation, $j_{gas} \sim j_c$ – a clear signature that the disc completely dominates the kinematics in this region.

We now turn to the main mechanism of angular momentum loss by the gas. If angular momentum were conserved during the collapse, the gas within the dominant DM halo potential would be able to collapse only by a factor of ~ 10 before forming a disc (e.g. Shlosman 2013, and references therein). However, the shapes of growing DM haloes are inherently triaxial, as seen in virtually all numerical simulations (e.g. Allgood et al. 2006; Berentzen, Shlosman & Jogee 2006). The gravitational torques which result from such haloes remove angular momentum from the gas and allow the collapse to proceed (e.g. Berentzen & Shlosman 2006). This happens even in regions where the gas has decoupled from the DM, because for non-axisymmetric mass distributions, the external mass can impose torques on smaller radii.

We have verified the importance of gravitational torques on large and small spatial scales in cosmological simulation of direct collapse (Choi et al. 2015). On larger scales, $r \sim 10$–50 pc, we have extended this analysis for another ~ 10 Myr, in the presence of the massive central seed (Fig. 11, left frame). A careful inspection of this region shows that the high amplitude of the $m = 2$ mode has its origin in a pair of dominant filaments, which feed the outer disc at a high mass accretion rate. So, indeed, the development of the $m = 2$ mode with some non-negligible amplitude is expected here. Prior to the formation of the central seed, the gas on these scales responds to the torques from the DM halo, and its response is that of a self-gravitating fluid. However, after $t \sim 362$ Myr, the radius of influence of the seed is about $r_{infl} \sim 43 \, M_{seed,6} v_{vir,10}^{-2}$ pc, where $M_{seed,6}$ is the seed mass in units of $10^6 \, M_{\odot}$, and $v_{vir,10}$ is the DM halo virial velocity in units of $10 \, km \, s^{-1}$. Hence, almost immediately after its formation, the central seed dominates the dynamics of the region hosting the discs. After this time, the gas response to the external torques, both hydrodynamical and gravitational, is that of a non-self-gravitating fluid.

The morphological evolution of the outer disc is, therefore, dominated by the mass influx along the filaments. Without this perturbation, the disc would become largely axisymmetric, but as the deprojected image of the face-on outer disc shows (Fig. 11, middle frame), it is dominated by spiral modes, from $m = 2$ to higher harmonics, with substantial amplitudes. The inner disc, within a cylindrical annulus $0.5 \lesssim r \lesssim 2$ pc, and thickness $\Delta z = 0.5$ pc, exhibits a lower amplitude $m = 2$ and 1 responses (Fig. 11, right frame), and is affected by the filaments to a smaller extent. Note that the misalignment of the two discs itself can in principle produce gravitational torques and induce $m = 2$ density modes, albeit heavily diluted by the central seed.

Thus, the self-gravity of both discs is severely diluted by the gravity of the massive seed in the centre. The outer disc is perturbed by the pair of external filaments which maintains the $m = 2$ symmetry there. The inflow rate that reaches the inner disc is much smaller, comes mostly from the outer disc (with infall along the rotation axis), and appears more axially symmetrized.

How stable is the configuration of misaligned discs and why did it form in the first place? The answer to the latter question is that the misaligned discs form in response to the variable angular momentum axis in the accretion flow. Future simulations will show whether this configuration is limited to a pair of discs, or whether additional misaligned rotating flows can form at larger radii. The reason for its apparent stability is found in the two filaments which feed the outer disc. By the end of the simulation, $t \sim 369.12$ Myr, these filaments have been substantially degraded, and so one can expect that the discs will re-align themselves. But gravitational torques between the discs are severely diluted by the central seed, which helps to prolong the life of this configuration. Of course, continuing collapse will add additional mass to the region, and one cannot predict a priori what will be the direction of its angular momentum vector.

To summarize, the massive seed fundamentally transforms the character of the accretion flow, to a large extent independently of the numerical resolution, once the radius of influence of this seed is resolved. Most importantly, as long as it dominates gravitationally, the massive seed dilutes the self-gravity of the gas, damps
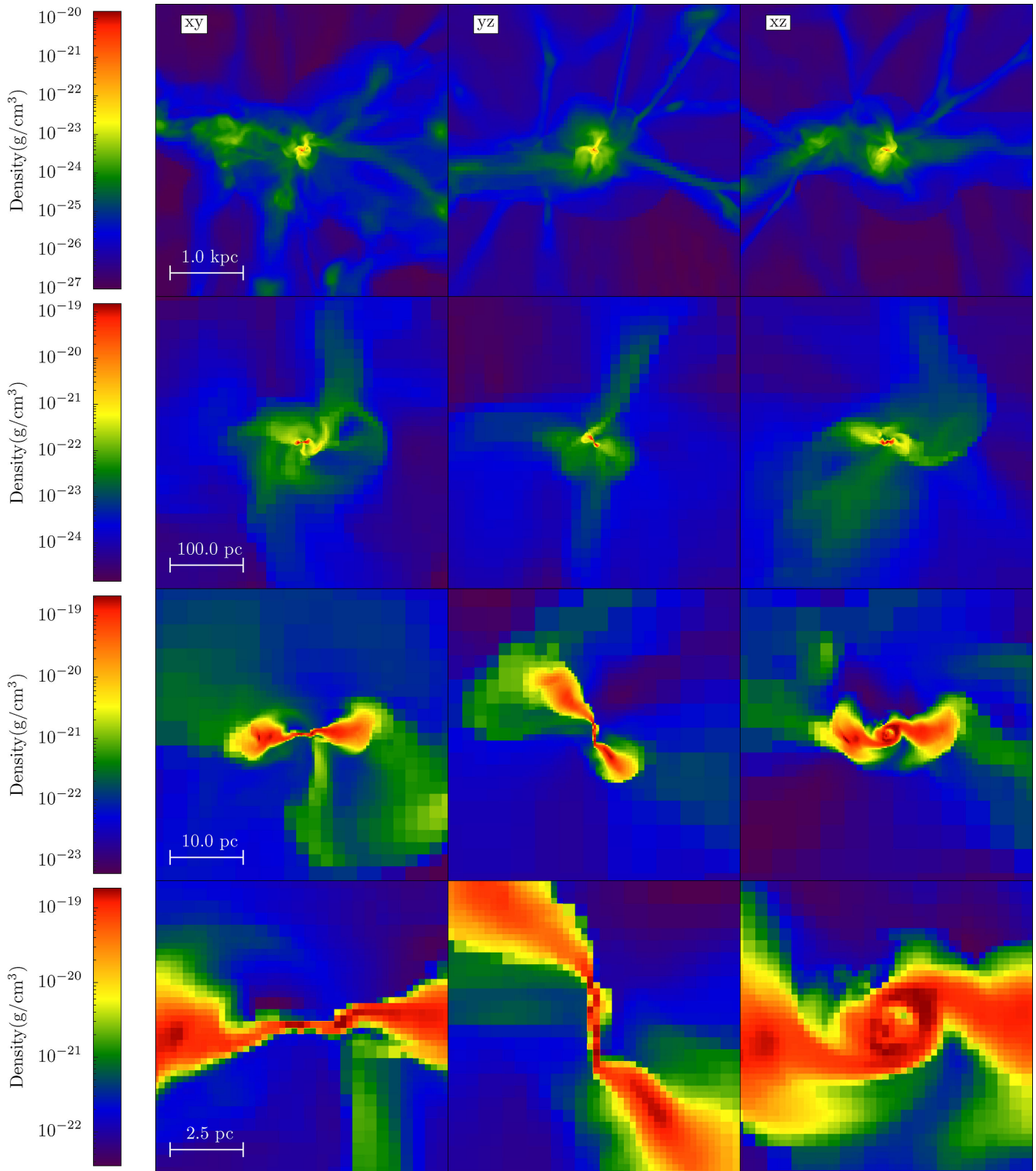
Figure 8. Gas density slices in three projections at the end of the simulation, $t \sim 369$ Myr, for run L12. The frames spanning 40 and 10 pc (on a side) exhibit prominent disc features with the *xy* and *yz* planes displaying nearly edge-on views, and the *xz* plane showing a nearly face-on view of the forming disc around the most massive sink particle.

fragmentation, decreases substantially the angular momentum transfer away from the gas, and, therefore, leads to the formation of a disc(s) in its vicinity. The scale chosen to break the self-similar collapse in our runs, given by the condition to create sink parti-

cles, determines the position of the discy flow at ~ 0.01–10 pc. Increasing or decreasing this scale would move the disc inwards or outwards, respectively, but the appearance of such a flow is generic.
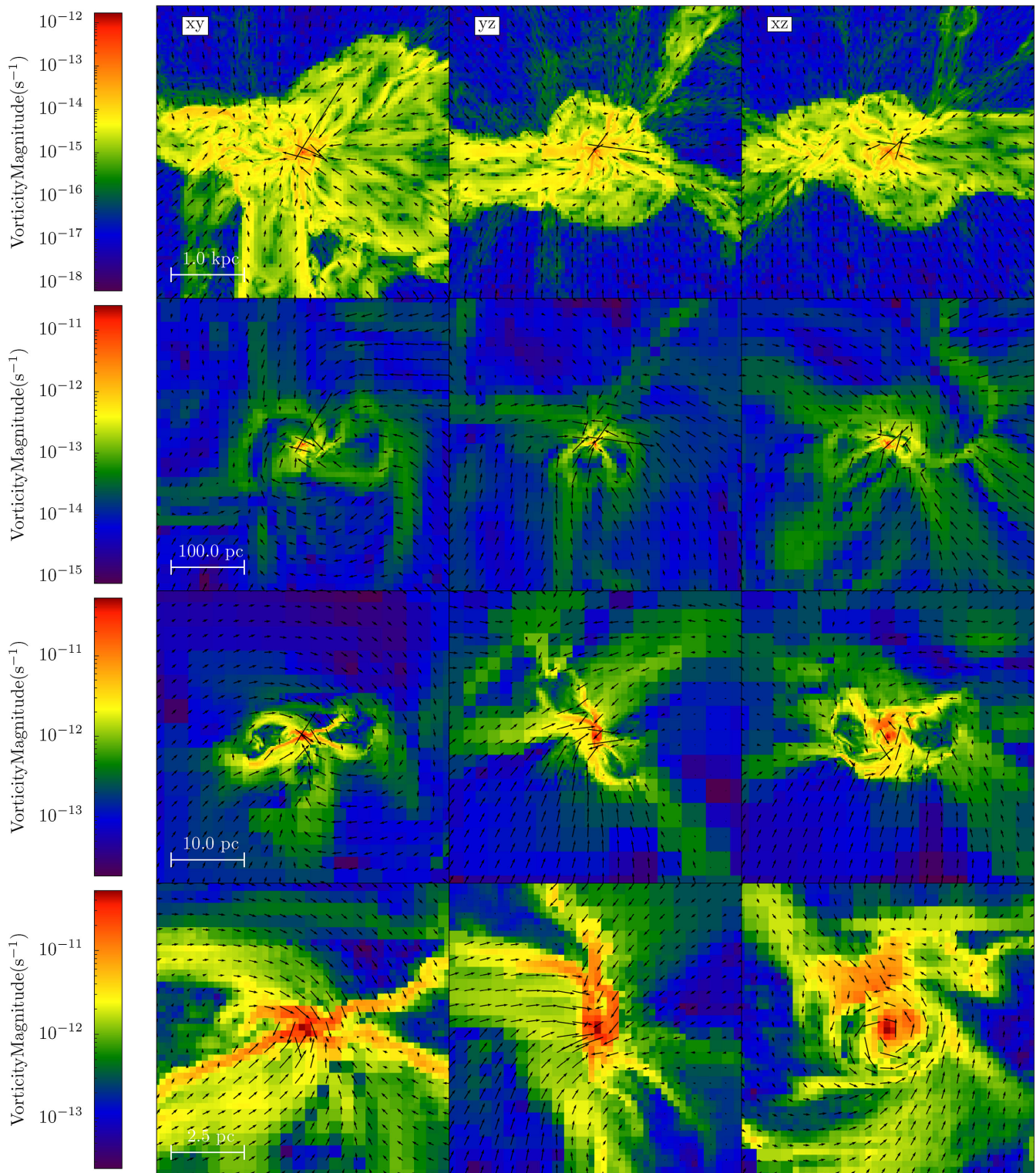
Figure 9. Vorticity magnitude slices of the gas evolution with projected velocity arrows, at the end of the simulation, $t \sim 369$ Myr, for run L12. Velocity arrows confirm the dominant rotation in the *xz* plane. Arrows in the *xy* and *yz* planes show a shock forming at the disc surfaces in the gas which is accreted from outside the disc plane.

3.4 Evolution of turbulent motions in the accretion flow

It is more difficult to recognize the two-disc system in the vorticity magnitude slices displayed in Fig. 9. Nevertheless, the face-on and edge-on inner disc appears prominent in the *yz* and *xz* projection planes in the bottom frames. For the edge-on projections of this disc, one observes accretion flows that are directed along its rotation axis. These flows appear to be highly turbulent. Generally, the vorticity increases towards the centre, as the vorticity maps show on various
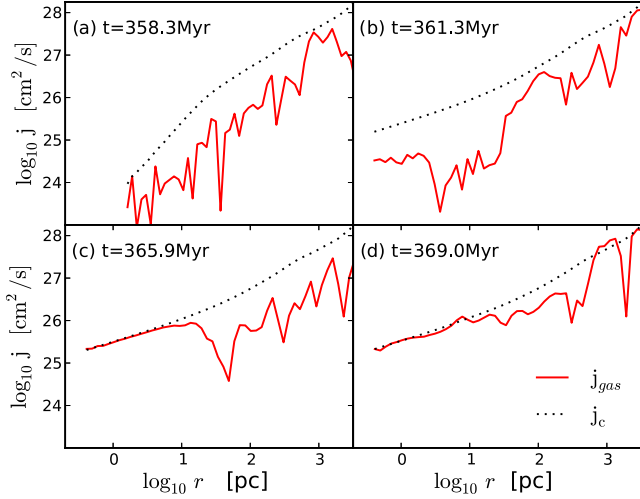
Figure 10. Evolution of the specific angular momentum profile in the gas, $j(r)$, for run L12 at 358.3 Myr (top left), 361.33 Myr (top right), 365.9 Myr (bottom left), and 369.0 Myr (bottom right). The angular momentum is measured in a cylindrical volume with a thickness of 10 pc, with respect to the rotation axis of the inner disc, which happens to nearly coincide with the y-axis of the computational box. The dotted lines represent the instantaneous Keplerian specific angular momentum profiles. Note that the innermost j_{gas} reaches its Keplerian value at later times.

spatial scales. The flow is turbulent both away from the outer disc and in its vicinity, though closer to the outer disc mid-plane the turbulence decays. Further analysis of the developing turbulence in the collapsing flow will be presented elsewhere.

4 DISCUSSION

We have used cosmological zoom-in simulations with the AMR ENZO code to study the long-term evolution of direct collapse that can lead to the formation of SMBH seeds at high redshifts. To circumvent the Courant condition on the timestep we have invoked the sink particle method. Sink particles are introduced when the refinement criterion has been violated and the resolution becomes insufficient at the highest refinement level (see Section 2). The innermost accretion flow on scales of $\lesssim 1$ pc forms a number of sink particles after ~ 361.5 Myr. They have been permitted to grow by

accretion and merging. By comparing various spatial resolutions, we find that allowing for a maximum of 12 refinements, corresponding to 0.1 pc resolution, is sufficient to obtain the convergence in the growth rate of the central sink particle, i.e. this growth rate remains unchanged when the resolution is increased. Under these conditions, we have been able to prolong the evolution of the collapsing gas by another 10 Myr, compared to Choi et al. (2015), who stopped the simulations at $t = 360.13$ Myr ($z \sim 12$) after the big bang. Our main results show that

(i) The masses of these sink particles have remained below $\sim 10^3$ M$_\odot$, with the exception of the central particle which grows rapidly to $M_{seed} \sim 2 \times 10^6$ M$_\odot$ in less than ~ 2 Myr, due to gas accretion and merging with other particles.

(ii) This growth coincides with the cessation of gravitational collapse on sub-pc scales and the formation of two misaligned gas discs – the inner one after ~ 361.5 Myr and the outer one after ~ 363.7 Myr.

(iii) Formation of misaligned discs is related to the variability of the angular momentum direction in the region.

(iv) As we discuss below (see also Section 3.2), the appearance of the massive object (hereafter central seed) in the centre is responsible for the cutoff of collapse.

(v) On larger scales, however, the collapse continues unimpeded. At this point, we make no assumptions about the nature of this massive object, but note that its rapid formation confirms the feasibility of this path to an SMBH.

We have analysed the co-evolution of the flow with the growth of the central seed, on scales comparable to the size of the forming disc. For this purpose, we have computed the evolution of Fourier modes on scales ~ 0.5–2 pc in the inner disc, 2.5–10 pc in the outer disc, and 10–50 pc outside the disc system. The low $m = 1$ to 3 mode amplitudes remain moderate, in the range of 0.2–0.4 (relative to $m = 0$) in the inner disc, and the outer disc is dominated by $m = 2$ spiral modes. They do not show any additional growth which can be expected if the fluid is self-gravitating. In both discs, we estimate that gas self-gravity is not important in comparison with the gravitational acceleration due to the massive central seed, and show that the fragmentation in the discs is damped due to the sharp increase of the Jeans masses there, after the formation of the massive seed (Section 3.2). In other words, the discs lie within the Roche limit of the central seed. However, the inflow into
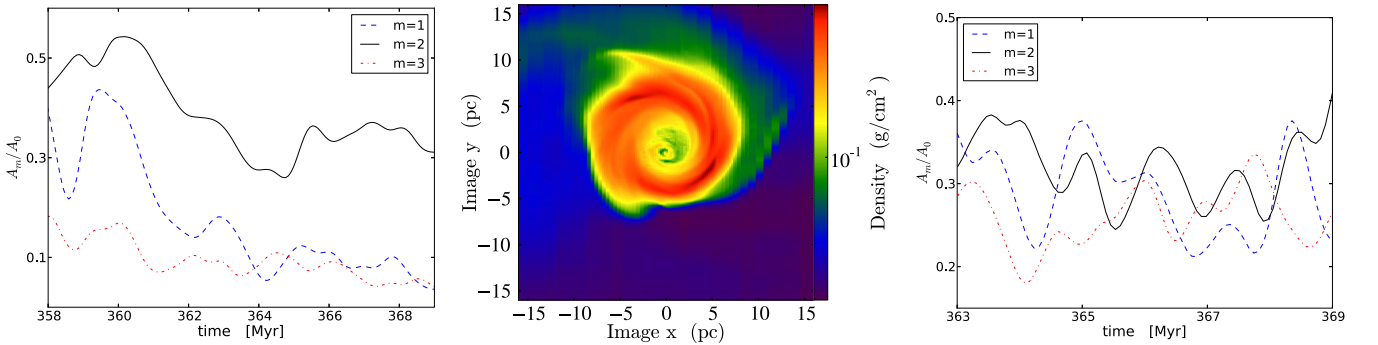

Figure 11. Evolution of the non-axisymmetric modes on progressively smaller spatial scales – in the region dominated by the filaments, and in the outer and inner discs. Left: evolution of the Fourier gas density modes $m = 1, 2$, and 3, normalized to the $m = 0$ mode amplitude for run L12 in the penetrating filaments region. The amplitudes are measured within the cylindrical annulus defined by $r \sim 10$–50 pc and thickness $\Delta z = 10$ pc. Middle: face-on outer disc and inclined inner disc at the end of the simulation, $t = 369.12$ Myr. Note the effect of the outer filaments penetrating the disc and driving $m = 2$ and higher modes in the form of spirals. Right: evolution of the Fourier gas density modes $m = 1, 2$, and 3, normalized to the $m = 0$ mode amplitude for run L12 in the face-on inner disc. The amplitudes are measured within the cylindrical annulus defined by $r \sim 0.5$–2 pc and thickness $\Delta z = 0.5$ pc.

the outer disc is dominated by a pair of filaments which maintain the $m = 2$ perturbation for a long time, while shear tends to axisymmetrize it. The mass inflow there is high, $\dot{M} \sim 0.3\,\mathrm{M}_\odot\,\mathrm{yr}^{-1}$. The inner disc is fed at a much smaller rate, $\dot{M} \lesssim 10^{-2}\,\mathrm{M}_\odot\,\mathrm{yr}^{-1}$, by the outer disc. Under these conditions of severely diluted self-gravity, mode coupling does not operate and the non-axisymmetric (and mostly $m = 2$) modes quickly saturate (e.g. Christodoulou, Shlosman & Tohline 1995).

Because the innermost accretion rate is substantially below that on larger spatial scales, the gas will accumulate in the disks, as discussed in Section 3.2 and shown in Fig. 2. We expect that this mass growth can lead to some local gravitational instabilities in the discs, but not to the resumption of a massive accretion on to the central seed.

A number of important issues are related to this evolution. Probably the most interesting one is how the collapse proceeds on smaller scales – this has been deliberately ignored in the current work, with the introduction of the seed particle algorithm. We anticipate that the cessation of the accretion process observed here justifies our conclusion that the characteristic mass of the forming SMBH seed is $M_\bullet \sim 10^6\,\mathrm{M}_\odot$.

Another issue is related to the fate of the inclined discs configuration, which formed as a result of gas flowing into the region with a variable orientation of angular momentum. Most probably this configuration will be destroyed by the same process that created it in the first place. In any case, if the SMBH seed forms before the next spike in the accretion rate, the radiation and/or mechanical feedback could already modify substantially the conditions in the inflowing gas.

The presence of the massive central object can be favourable for the growth of the $m = 1$ mode in the surrounding accretion disc, when the disc mass is *not* negligible compared to the massive object – hence when disc self-gravity is not severely diluted by the object (e.g. Adams, Ruden & Shu 1989). Furthermore, for *stellar* discs, which are dominated by the central object and hence reside in the Keplerian potential, the $m = 1$ mode, when triggered, can be long-lived, due to the absence of precession in this potential (Tremaine 1995). Under these conditions, the individual stellar orbits can be weakly 'glued' by their gravitational attraction and can maintain this non-axisymmetric mode. This mode has been suggested to be responsible for the mass accretion rate on to the SMBH under certain conditions (Hopkins & Quataert 2010).

However, one expects that the $m = 1$ mode will not be able to grow when strong time-dependent perturbations are present, which destroy the orbital correlations in the Keplerian gaseous disc, i.e. in a disc with the ratio of the central mass-to-disc mass much greater than unity. We do not observe any substantial growth of $m = 1$ mode and any mass accretion flux associated with this mode.

Fast growth of the central object will have dynamical consequences for the collapsing flow. Among these, the most important appears to be the *inability* of the flow to get rid of its angular momentum. Gravitational torques from the DM serve as the main mechanism extracting angular momentum from the gas, but close to the massive central seed, the torques are diluted by the gravitational monopole and become inefficient. The gas acquires rotational support and settles in a disc-like configuration around the centre. Its fragmentation is damped by the tidal forces of the central seed in the presence of the floor temperature of atomic gas.

Damping of the non-axisymmetric instabilities in the disc leads to the inability of the gas to transfer its angular momentum to the outer gas or to the surrounding DM. This results in the accumulation of gas in this region and the growth of the disc. In fact, the rapid growth of the central object is the prime cause of the formation of the discs on these scales and of their lack of fragmentation. After the initial period of rapid growth, the massive central object continues to grow but at a much slower pace, by a factor of $\sim$2–3 (Fig. 1).

The corollary of this evolution is the formation of a massive object in the centre of the direct collapse region. The resolution scale in our model is chosen somewhat arbitrarily, just to allow for the second stage of the collapse to be resolved spatially. But our results bring up an important issue: How does the nature of the accretion flow changes with the formation and growth of the central massive object? The resulting formation of the gaseous disc around this object is a direct consequence of dramatically reduced efficiency of angular momentum transfer within the radius of influence of the massive centre, R_{infl} (Section 3.3). Of course, the compactness parameter of such an object, $M_{\mathrm{seed}}/R_{\mathrm{seed}}$, where R_{seed} is the seed size, will determine the inner edge of the forming disc, but not the position of its outer edge, as long as it is resolved numerically. Here R_{seed} is the size of the seed or the associated numerical resolution.

We have also assumed that the molecular gas, H_2, is not present during direct collapse, and, therefore, the floor temperature of the atomic gas lies around a several thousand degrees. We justify this by the presence of the Lyman–Werner continuum which originates in nearby stellar populations (e.g. Agarwal & Khochfar 2015) or *in situ* (Choi et al. 2013).

Another important issue is our neglect of the radiation feedback in the region of the disc. To address this, it is crucial to know the nature of the massive object, and the source of the radiation field. If this object is an SMS fuelled by the thermonuclear reactions in the core and accretion energy in the envelope (e.g. Begelman 2010), this will specify the effective temperature, spectral energy distribution and geometry of the radiation field. Alternatively, if the SMS stage is bypassed (see Section 1), the rate of locally produced energy will be very different and the radiation field could become anisotropic, with most of it escaping in the preferred direction, i.e. the rotation axis. We also note that very large accretion rates encountered during direct collapse can make the radiation feedback much less efficient dynamically.

REFERENCES

Abel T., Anninos P., Zhang Y., Norman M. L., 1997, New Astron., 2, 181
Abel T., Bryan G. L., Norman M. L., 2002, Science, 295, 93
Adams F. C., Ruden S. P., Shu F. H., 1989, ApJ, 347, 959
Agarwal B., Khochfar S., 2015, MNRAS, 446, 160

Allgood B., Flores R. A., Primack J. R., Kravtsov A. V., Wechsler R. H., Faltenbacher A., Bullock J. S., 2006, MNRAS, 367, 1781

Anninos P., Zhang Y., Abel T., Norman M. L., 1997, New Astron., 2, 209

Bate M. R., Bonnell I. A., Price N. M., 1995, MNRAS, 277, 362

Becerra F., Greif T. H., Springel V., Hernquist L. E., 2015, MNRAS, 446, 2380

Begelman M. C., 2010, MNRAS, 402, 673

Begelman M. C., Shlosman I., 2009, ApJ, 702, L5

Begelman M. C., Volonteri M., Rees M. J., 2006, MNRAS, 370, 289

Berentzen I., Shlosman I., 2006, ApJ, 648, 807

Berentzen I., Shlosman I., Jogee S., 2006, ApJ, 637, 582

Berger M. J., Colella P., 1989, J. Comput. Phys., 82, 64

Bromm V., Larson R. B., 2004, ARA&A, 42, 79

Bromm V., Loeb A., 2003, ApJ, 596, 34

Bryan G. L., Norman M. L., 1997, in Clarke D. A., West M. J., eds, ASP Conf. Ser. Vol. 123, Computational Astrophysics; 12th Kingston Meeting on Theoretical Astrophysics. Astron. Soc. Pac., San Francisco, p. 363

Bryan G. L., Norman M. L., Stone J. M., Cen R., Ostriker J. P., 1995, Comput. Phys. Commun., 89, 149

Bryan G. L. et al., 2014, ApJS, 211, 19

Choi J.-H., Shlosman I., Begelman M. C., 2013, ApJ, 774, 149

Choi J.-H., Shlosman I., Begelman M. C., 2015, MNRAS, 450, 4411

Christodoulou D. M., Shlosman I., Tohline J. E., 1995, ApJ, 443, 551

Eisenstein D. J., Hut P., 1998, ApJ, 498, 137

Fan X. et al., 2003, AJ, 125, 1649

Federrath C., Banerjee R., Clark P. C., Klessen R. S., 2010, ApJ, 713, 269

Federrath C., Sur S., Schleicher D. R. G., Banerjee R., Klessen R. S., 2011, ApJ, 731, 62

Gong H., Ostriker E. C., 2013, ApJS, 204, 8

Haehnelt M. G., Rees M. J., 1993, MNRAS, 263, 168

Hahn O., Abel T., 2011, MNRAS, 415, 2101

Haiman Z., Loeb A., 2001, ApJ, 552, 459

Hopkins P. F., Quataert E., 2010, MNRAS, 407, 1529

Hosokawa T., Omukai K., Yoshida N., Yorke H. W., 2011, Science, 334, 1250

Inayoshi K., Omukai K., Tasker E., 2014, MNRAS, 445, L109

Johnson J. L., Khochfar S., Greif T. H., Durier F., 2011, MNRAS, 410, 919

Krumholz M. R., McKee C. F., Klein R. I., 2004, ApJ, 611, 399

Latif M. A., Zaroubi S., Spaans M., 2011, MNRAS, 411, 1659

Latif M. A., Schleicher D. R. G., Schmidt W., Niemeyer J., 2013, MNRAS, 433, 1607

Li Y. et al., 2007, ApJ, 665, 187

Mayer L., Kazantzidis S., Escala A., Callegari S., 2010, Nature, 466, 1082

Milosavljević M., Bromm V., Couch S. M., Oh S. P., 2009, ApJ, 698, 766

Mortlock D. J. et al., 2011, Nature, 474, 616

Navarro J. F., Frenk C. S., White S. D. M., 1997, ApJ, 490, 493

Norman M. L., Bryan G. L., 1999, Astrophys. Space Sci. Libr., 240, 19

Oh S. P., Haiman Z., 2002, ApJ, 569, 558

Omukai K., 2001, ApJ, 546, 635

Pelupessy F. I., Di Matteo T., Ciardi B., 2007, ApJ, 665, 107

Planck Collaboration XIII 2015, preprint (arXiv:1502.01589)

Prieto J., Jimenez R., Haiman Z., 2013, MNRAS, 436, 2301

Schleicher D. R. G., Spaans M., Glover S. C. O., 2010, ApJ, 712, L69

Shlosman I., 2013, in Falcón-Barroso J., Knapen J. H., eds, Secular Evolution of Galaxies. Cambridge Univ. Press, Cambridge, p. 555

Spaans M., Silk J., 2006, ApJ, 652, 902

Sugimura K., Omukai K., Inoue A. K., 2014, MNRAS, 445, 544

Sur S., Schleicher D. R. G., Banerjee R., Federrath C., Klessen R. S., 2010, ApJ, 721, L134

Teyssier R., Moore B., Martizzi D., Dubois Y., Mayer L., 2011, MNRAS, 414, 195

Tremaine S., 1995, AJ, 110, 628

Truelove J. K., Klein R. I., McKee C. F., Holliman J. H., II, Howell L. H., Greenough J. A., 1997, ApJ, 489, L179

Turk M. J., Oishi J. S., Abel T., Bryan G. L., 2012, ApJ, 745, 154

Turk M. J., Smith B. D., Oishi J. S., Skory S., Skillman S. W., Abel T., Norman M. L., 2011, ApJS, 192, 9

Volonteri M., Rees M. J., 2006, ApJ, 650, 669

Wang P., Li Z.-Y., Abel T., Nakamura F., 2010, ApJ, 709, 27

Wise J. H., Turk M. J., Abel T., 2008, ApJ, 682, 745

Wu X.-B. et al., 2015, Nature, 518, 512

This paper has been typeset from a TEX/LATEX file prepared by the author.